Indian J Phys (August 2019) 93(8):979–989
https://doi.org/10.1007/s12648-018-01365-8

ORIGINAL PAPER

Pressure-induced phase transitions, electronic, elastic and vibrational properties of zinc oxide under high pressure

C Kürkçü[1,3]*, Z Merdan[2,3] and Ç Yamçıçıer[2,3]

[1]Department of Electronics and Automation, Ahi Evran University, 40100 Kırşehir, Turkey

[2]Science Faculty, Gazi University, 06500 Ankara, Turkey

[3]Institute of Science, Gazi University, 06500 Ankara, Turkey

Received: 31 May 2018 / Accepted: 25 September 2018 / Published online: 17 January 2019

Abstract: In this work, the crystal structure of the ZnO was studied under high hydrostatic pressure using ab initio calculations. Pressure–volume relationships and structural transitions in ZnO were investigated using Siesta method. A first-order transition from the hexagonal wurtzite (B4) structure with space group $P6_3mc$ to the cubic NaCl (B1) structure with space group $Fm\bar{3}m$ was successfully observed. A transition was also observed from $Fm\bar{3}m$ to another cubic CsCl (B2) structure with space group $Pm\bar{3}m$ for ZnO. These phase transitions which occur around 9 and 119.5 GPa were also analyzed from the total energy and enthalpy calculations. In addition, electronic, elastic and vibrational properties of ZnO were analyzed based on the high pressure.

Keywords: Phase transitions; Electronic structure calculations; Pressure; Bulk crystals

PACS Nos.: 64.60.−I; 71.15.−m; 61.50.Ks; 61.50.−f

1. Introduction

Recently, the properties of ZnO have been subject to many experimental and theoretical studies in recent years due to its technological significance in various fields including photovoltaic, piezoelectric surface acoustic wave devices, varistors, optical waveguides, gas sensors, ceramics, etc. [1–14]. For example, ZnO films are used as n-type conductive glass in thin-film solar cells consisting of copper indium diselenide [1] or amorphous silicon [2]. It is a low-cost material well adapted for the new generation of solar cells.

Besides the above-mentioned properties, the high-pressure behavior of ZnO has theoretically attracted interest at the same time [14–17]. There is a continuing interest in the high-pressure behavior of ZnO in the field of geophysics as well as the basic material physics [13]. The phase-dependent phase transition in ZnO has been studied experimentally and theoretically. Experimental studies have shown that the B4 phase of ZnO is converted to the B1 phase at about 10 GPa [18], and then, this transformation is performed by Jamieson [19] and Yu et al. [20]. Desgreniers reported that the transition pressure (Pt) for B4 → B1 transition was 9.1 ± 0.2 GPa and a 16.7% collapse in volume [21]. Energy-diffused X-ray diffraction (EDX) studies have shown that the transition from B4 → B1 occurs at about 9.8 GPa at room temperature [22, 23]. In addition, previous high-pressure structural calculations have mostly focused on phase transformation from B4 to B1. The linear combination of Gaussian-type orbitals (LCGTO) Hartree–Fock (HF) method reported a transit pressure of 8.57 GPa [16]. The elastic and structural properties of ZnO have been investigated with the full-potential linear-muffin-tin-orbital method (FP-LAPW) [24].

Recently, the structural parameters of ZnO in three phases (B4, B1, B3), as well as the transition to B1 and B3 phases from B4, have been presented with both the local density approximation (LDA) and the generalized gradient approximation (GGA) [25].

We also investigated the electronic properties of ZnO for low- and high-pressure phases and found that all phases of ZnO exhibited semiconducting properties.

*Corresponding author, E-mail: ckurkcu@ahievran.edu.tr

Table 1 Theoretical (T = 0 K) lattice parameters of ZnO for wurtzite structure (space group, SG:$P6_3mc$) and high-pressure phases: Rock-salt structure (SG:$Fm\bar{3}m$) and CsCl structure (SG:$Pm\bar{3}m$) with GGA at the corresponding pressure P_T. a, b and c are the lattice parameters, V is the equilibrium volume at the respective pressure, B_0 the bulk modulus, B_0' the first derivative of the bulk modulus

Phases	P (GPa)	a (Å)	b (Å)	c (Å)	V (Å)	B_0 (GPa)	B_0'	References
$P6_3mc$	0	3.2896	3.2896	5.2829	49.51	168.43	4.17	This study
		3.1900	3.1900	5.1800	49.18	146.00		[7]
		3.2562	3.2562	5.2563				[8]
		3.1950	3.1950	5.1200		161.60	4.53	[9]
		3.2890	3.2890	5.3080		128.20		[10]
		3.2077	3.2077	5.1636	46.00	168.40	4.34	[11]
		3.1832	3.1832	5.1482	45.16	164.36	3.77	[12]
		3.1841	3.1841	5.1550		145.90	3.72	[13]
$Fm\bar{3}m$	9.00	4.1746	4.1746	4.1746	72.75	201.84	4.49	This study
	9.00	4.2300	4.2300	4.2300	79.90	223.00		[7]
	13.0	4.2120	4.2120	4.2120				[8]
	9.48	4.2170	4.2170	4.2170		208.00	4.80	[9]
	8.72	4.3390	4.3390	4.3390		165.00		[10]
	8.08	4.2230	4.2230	4.2230	75.20	209.60	4.46	[11]
	10.49	4.2100	4.2100	4.2100	74.63	229.83	3.67	[12]
	8.80	4.2110	4.2110	4.2110		210.10	4.44	[13]
$Pm\bar{3}m$	119.50	2.3708	2.3708	2.3708	13.32	235.10	4.52	This Study
		2.6100	2.6100	2.6100	19.36	177.00		[7]
	251.00	2.6130	2.6130	2.6130		205.34	4.72	[9]
	268.50	2.6920	2.6920	2.6920		159.10		[10]
	243.53	3.2930	3.2930	3.2930	17.85	205.40	4.44	[11]
	260.00	2.6680	2.6680	2.6680	18.65	234.00	3.49	[12]
	263.00	2.6080	2.6080	2.6080		208.90	4.44	[13]

Table 2 The equilibrium lattice parameters and the atomic fractional coordinates of the $P6_3mc$, $Fm\bar{3}m$, and $Pm\bar{3}m$ phases

Phases	a (Å)	b (Å)	c (Å)	x	y	z
$P6_3mc$	3.2896	3.2896	5.2829	Zn: 0.3333	0.6667	0.5000
				Zn: 0.6667	0.3333	0.0000
				O: 0.3333	0.6667	0.1214
				O: 0.6667	0.3333	0.6214
$Fm\bar{3}m$	4.1746	4.1746	4.1746	Zn: 0.0000	0.0000	0.0000
				Zn: 0.0000	0.5000	0.5000
				Zn: 0.5000	0.5000	0.0000
				Zn: 0.5000	0.0000	0.5000
				O: 0.5000	0.5000	0.5000
				O: 0.5000	0.0000	0.0000
				O: 0.0000	0.0000	0.5000
				O: 0.0000	0.5000	0.0000
$Pm\bar{3}m$	2.3708	2.3708	2.3708	Zn: 0.0000	0.0000	0.0000
				O: 0.5000	0.5000	0.5000

The purpose of this article is to compare the structural and electronic properties of ZnO with other theoretical and experimental studies using the Siesta package program and to complement the lack of literature. The remainder of this article is organized as follows: Chapter 2 summarizes the calculation method, Chapter 3 results and discussion and Chapter 4 the conclusions.

2. The method of calculations

The phase transition properties of the hexagonal B4 structure of ZnO under pressure are investigated using the ab initio method. The SIESTA [26] package program is used as the ab initio code in the study. GGA approach is applied, and parameters of the Perdew–Burke–Ernzerhof (PBE) [27] exchange–correlation function are entered into the calculations with "double ζ (DZ) basis set." Troullier–Martins' norm-protective pseudo-potential [28] is used for electronic band structure, total and partial density of state calculations.

Cutoff energy at work is sufficient as 300 Ryd. In order to calculate the relation between the energy–volume, the

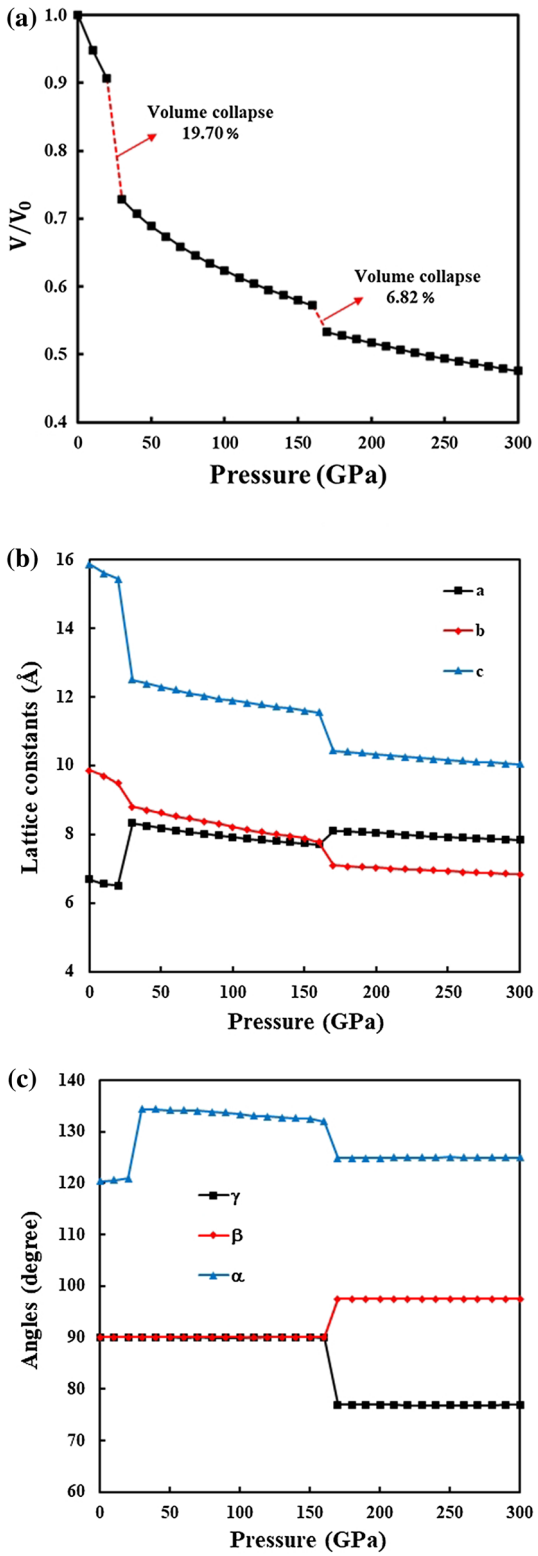

Fig. 1 (Color online) The graph of the change in simulation cell volume (**a**), lattice constant (**b**) and angles (**c**) as function of the pressure

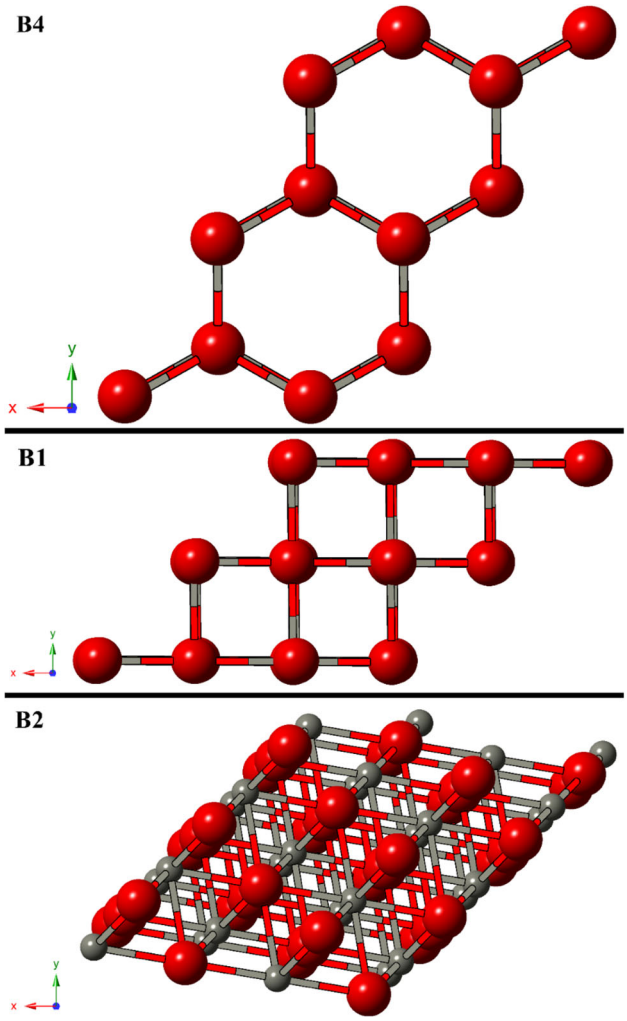

Fig. 2 (Color online) Crystal structures of ZnO: B4 at 0 GPa, B1 at 30 GPa and B2 at 170 GPa

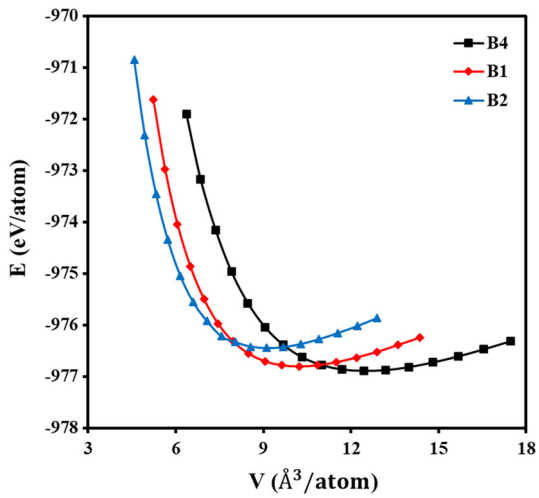

Fig. 3 (Color online) The energy–volume curves of the main structural phases of ZnO

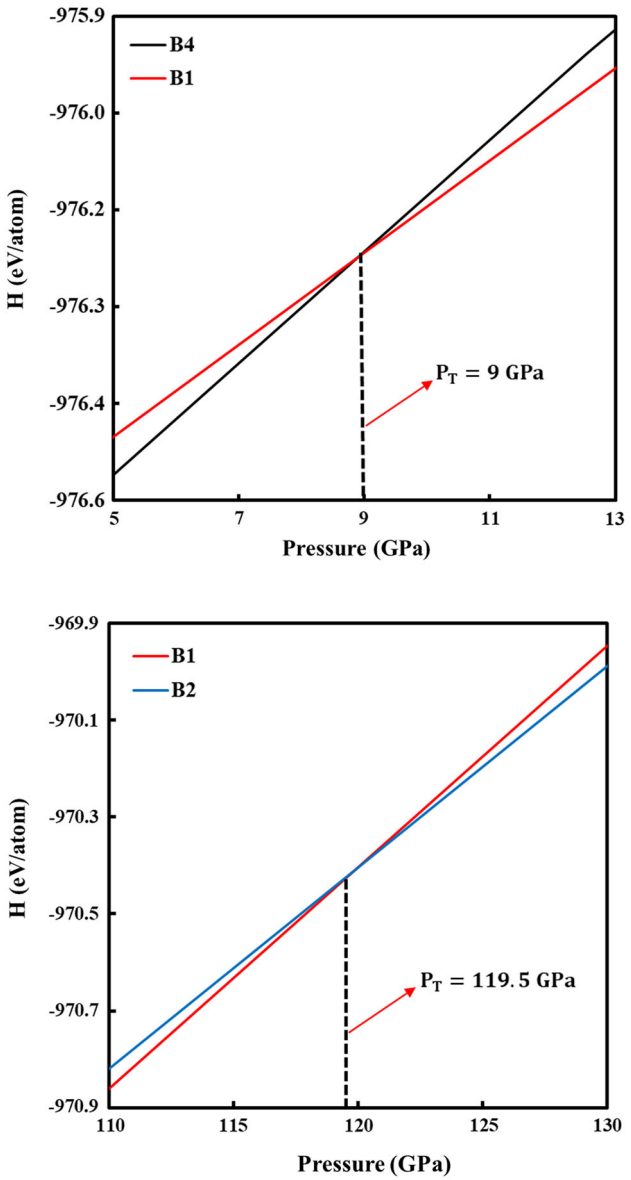

Fig. 4 (Color online) The enthalpy curves of the main structural phases of ZnO

unit cells of the crystal structures are utilized for $P6_3mc$, $Fm\bar{3}m$ and $Pm\bar{3}m$ structures.

For Brillouin region integration, 8 × 8 × 6, 8 × 8 × 8 and 8 × 8 × 8 Monkhorst–Pack (MP) mesh [29] were used for the $P6_3mc$, $Fm\bar{3}m$ and $Pm\bar{3}m$ structures, respectively. Simulation cells are constructed from 72 atoms under periodic bond conditions using a 3 × 3 × 2 supercell. Pressure is gradually increased by 10 GPa by applying conjugate gradient technique to the system. The KPLOT [30] program and the RGS [31] algorithm are used to analyze each simulation step. They give detailed information about the space group, atomic positions and lattice parameters of an analyzed structure. In addition, the Crystalmaker program is used to visualize phase transformation and its mechanism.

3. Results and discussions

Firstly, ZnO is equilibrated by relaxing 72 atoms supercell at zero pressure. The equilibrium unit cell lattice constants are found to be $a = b = 3.2896$ and $c = 5.2829$ Å for $B4$ structure. The transition pressure values, equilibrium lattice parameters, volume, bulk modulus and pressure derivatives of bulk modulus in Table 1 and the lattice parameters and fractional atomic positions in Table 2 are tabulated for ZnO.

As can be seen from Table 1, the obtained phase transition value for $Fm\bar{3}m \rightarrow Pm\bar{3}m$ is slightly lower than the other studies. ZnO crystallizes in two stable states under ambient conditions. One of these structures is hexagonal with space group $P6_3mc$, and the other is cubic with space group $Fm\bar{3}m$. Other authors preferred the $Fm\bar{3}m$ phase as the first phase and obtained phase transition from $Fm\bar{3}m$ to $Pm\bar{3}m$ at about 250 GPa. However, due to the lack of literature, we preferred the hexagonal phase as the first phase and obtained phase transitions from $P6_3mc$ to $Fm\bar{3}m$ at about 9 GPa and from this $Fm\bar{3}m$ phase to $Pm\bar{3}m$ phase at about 115.5 GPa. The pressure is gradually increased by 10 GPa by applying conjugate gradient technique to the system. The pressure of 10 GPa was applied to the structure of ZnO at 0 GPa. Then, a pressure of 20 GPa was applied to the structure obtained by applying pressure of 10 GPa. After that, pressure of 30 GPa was applied to the structure obtained by applying pressure of 20 GPa. In this way, when the pressure is gradually increased, the materials can undergo to phase transition at more low pressure. Because of this, while other authors observed the phase transition from $Fm\bar{3}m$ to $Pm\bar{3}m$ at about 250 GPa, we obtained this phase transition at about 115.5 GPa.

Later, the phase transition properties for ZnO are investigated under constant pressure. The pressure–volume relation is shown in Fig. 1. A sharp decrease in volume is observed because of the variation of the pressure from 20 to 30 GPa and from 160 to 170 GPa for $P6_3mc \rightarrow Fm\bar{3}m$ and $Fm\bar{3}m \rightarrow Pm\bar{3}m$, respectively. The collapse in the value of volume during this transformation shows us that the phase transition is first order.

Figure 2 shows that hexagonal B4 structure converts into a cubic B1 structure with space group $Fm\bar{3}m$ at 30 GPa, and then, this B1 structure converts into another cubic B2 structure with space group $Pm\bar{3}m$ at 170 GPa for ZnO. From the results, one can conclude that phase transitions of ZnO under pressure can be reliably predicted based on ab initio calculations. However, the predicted phase transition pressures give slightly different results

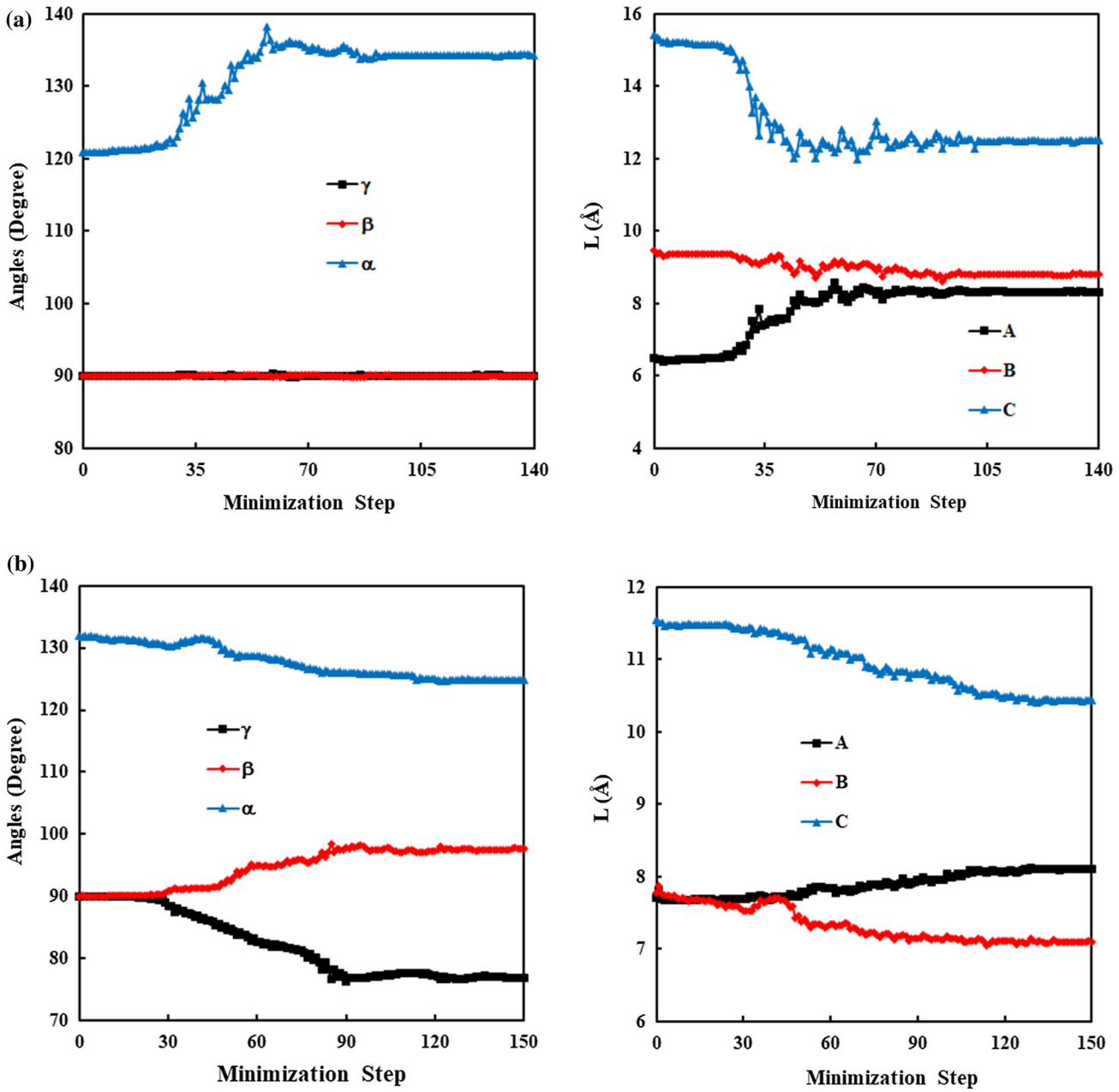

Fig. 5 (Color online) The behavior of the simulation cell lengths and angles as the function of minimization steps: **(a)** at 30 GPa and **(b)** at 170 GPa

compared with the experimental results. The reason of this difference is related to the infinite volume defect form of a free structure where the phase transition occurs over the whole simulation cell rather than nucleation and buildup. Therefore, such an overestimated transition pressure can be predicted for the particular conditions such as a finite size of the simulation cell and the time scale of simulations, etc. [32–36]. On the other hand, energy–volume calculations (see Fig. 3) are considered to find out the stability of B4, B1 and B2 structures, since the thermodynamic theorem does not consider the possible an activation energy barrier separating the two structural phases. As can be seen in Fig. 3, the most stable phase of ZnO is $P6_3mc$.

Their energy–volume data are fitted to the third-order Birch–Murnaghan equation of state [37, 38] that given by

$$P = 1.5B_0\left[\left(\frac{V}{V_0}\right)^{\frac{-7}{3}} - \left(\frac{V}{V_0}\right)^{\frac{-5}{3}}\right] x\left\{1 + 0.75\left(B_0' - 4\right)\left[\left(\frac{V}{V_0}\right)^{\frac{-2}{3}} - 1\right]\right\} \quad (1)$$

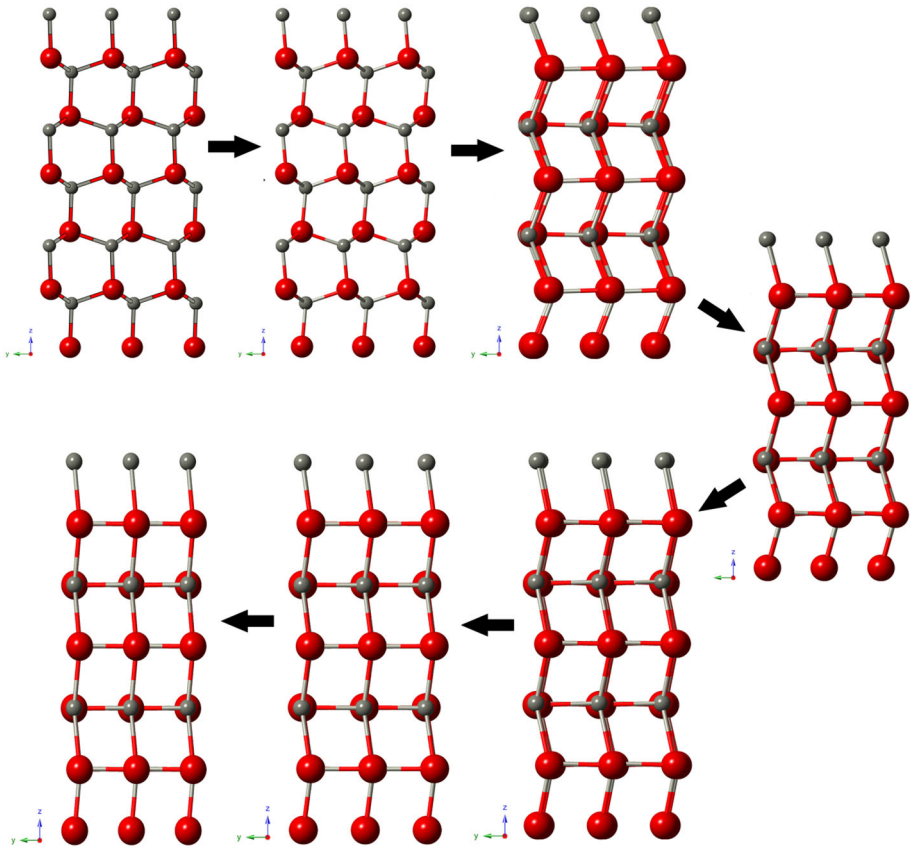

Fig. 6 (Color online) Formation of the B1 structure at 30 GPa

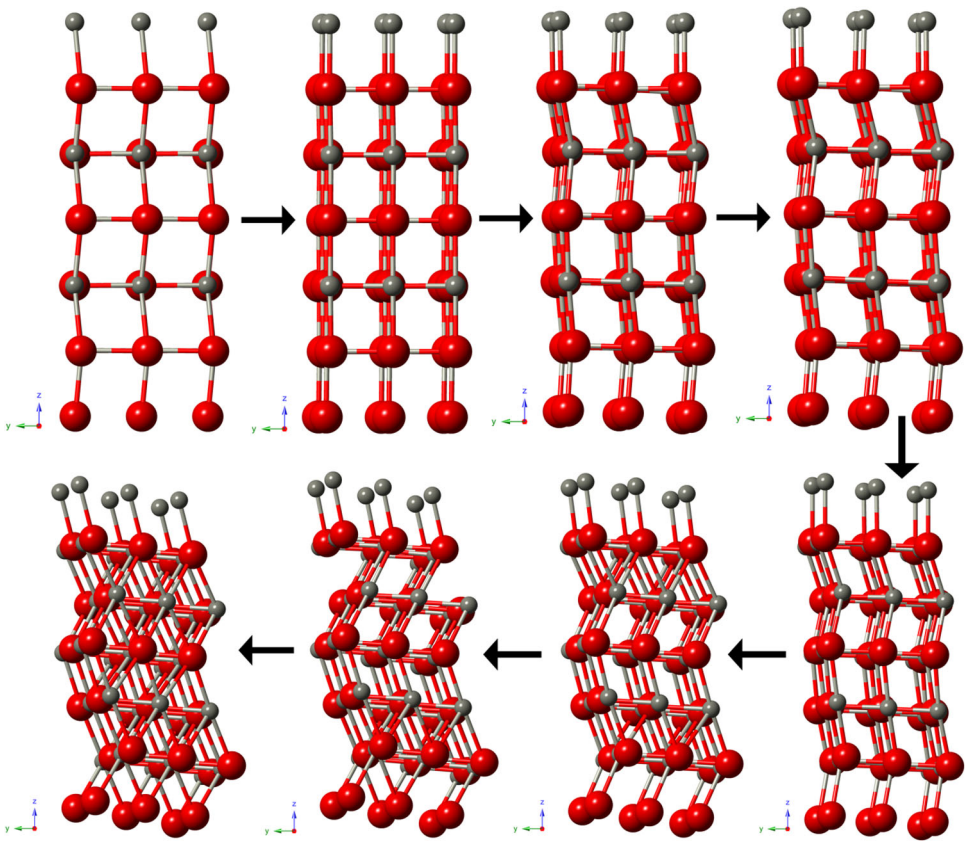

Fig. 7 (Color online) Formation of the B2 structure at 170 GPa

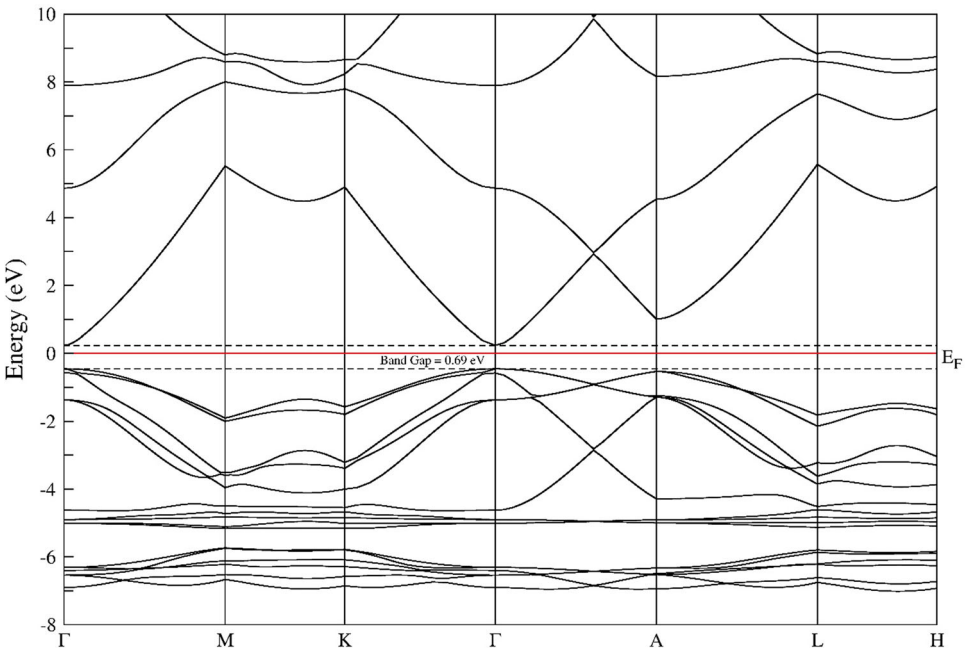

Fig. 8 Band structure for ZnO in the B4 structure at 0 GPa

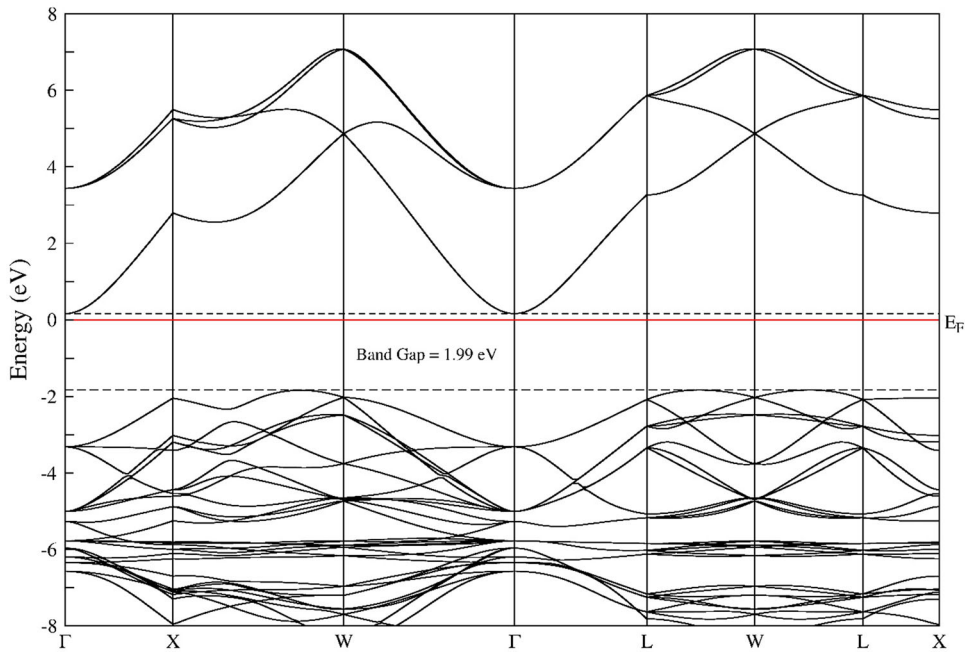

Fig. 9 Band structure for ZnO in the B1 structure at 30 GPa

where P is the pressure, V is the volume at the pressure, V_0, B_0 and $B_0^{'}$ are the volume, bulk modulus and its pressure derivate at 0 GPa, respectively.

Enthalpy (H) is the sum of the total energy (E_{tot}) and the product of pressure and volume (PV) given by the equation:

$$H = E_{\text{tot}} + PV \tag{2}$$

where $P = \mathrm{d}E_{\text{tot}}/\mathrm{d}V$ is obtained by differentiation of the predicted the energy–volume curves. Therefore, the transition pressure can be calculated by equating the enthalpy of the two pressure (see Fig. 4). The transition pressures about 9 and 119.5 GPa are obtained as $P6_3mc \rightarrow Fm\bar{3}m$ and $Fm\bar{3}m \rightarrow Pm\bar{3}m$, respectively.

The variation of the simulation cell under the pressure gives information about this transformation. The simulation box is initially a cubic cell whose lattice vectors are along the [0 0 1], [0 1 0] and [0 0 1] directions. Thus, as based on predicted parameters, we analyzed the variation

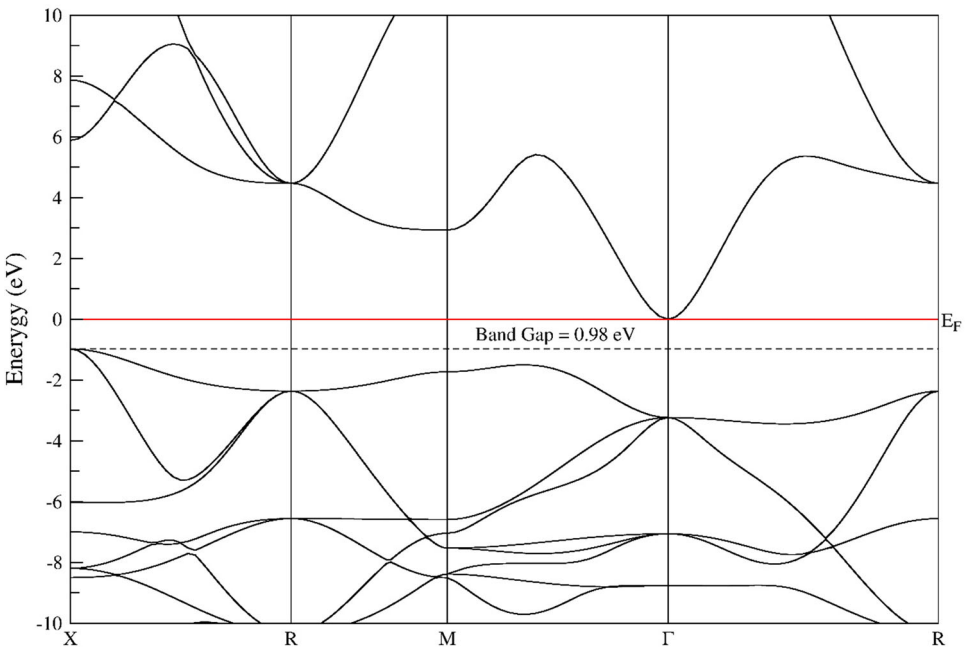

Fig. 10 Band structure for ZnO in the B2 structure at 170 GPa

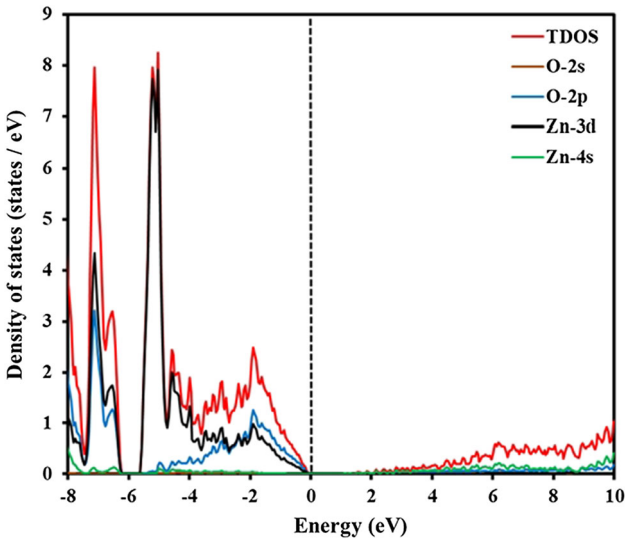

Fig. 11 The density of states for ZnO in the B4 structure at 0 GPa

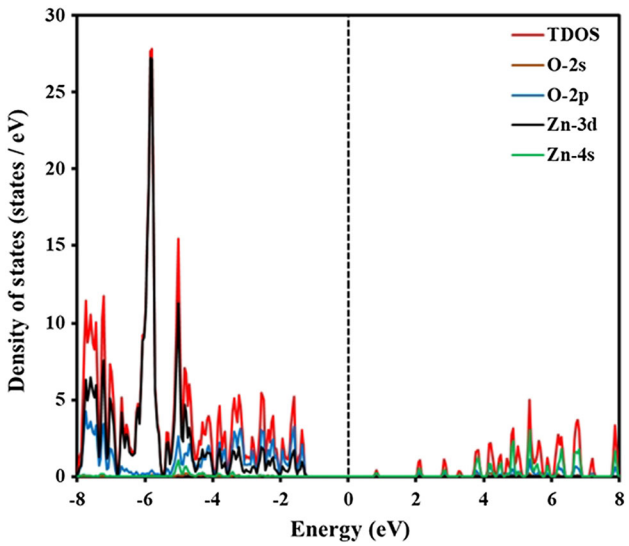

Fig. 12 The density of states for ZnO in the B1 structure at 30 GPa

of the simulation cell lengths and angles as a function of the minimization step (see Fig. 5).

From Fig. 5(a), the β and γ angles remain unchanged through the simulation, α angle starts to increase at around 60th minimization step, and after reaching about 135°, it remains unchanged through the simulation. The *A*, *B* and *C* remain constant up to about 50th minimization step. A increase up to about 8 Å, as *C* decreases up to about 12 Å. Then, they remain unchanged through the simulation.

As shown in Fig. 5(b), α and β angles remain unchanged through the simulation. γ angle remains constant up to about 30th minimization step. γ angle starts to decrease, and after reaching about 75°, it remains unchanged through the simulation. *B* and *C* decrease up to about 10.5 and 7 Å, respectively, as *A* remains constant through the simulation.

Each simulation step of the ZnO is analyzed in detail by the KPLOT program to determine whether there are any intermediate states during this phase change at 30 GPa and 170 GPa. As a result of the analysis, we suggest that the B1 phase of ZnO proceeds through five intermediate states with space groups $Cmc2_1$ at 17th step, *Cmcm* at 44th step, $P2_1/m$ at 51st step, *Pmmn* at 60th step and *I4/mmm* at 79th step. For the B2 phase, we suggest that it proceeds through six intermediate phases with space groups *Immm* at 15th step, *Cm* at 38th step, *P1* at 43rd step, *Pm* at 55th step,

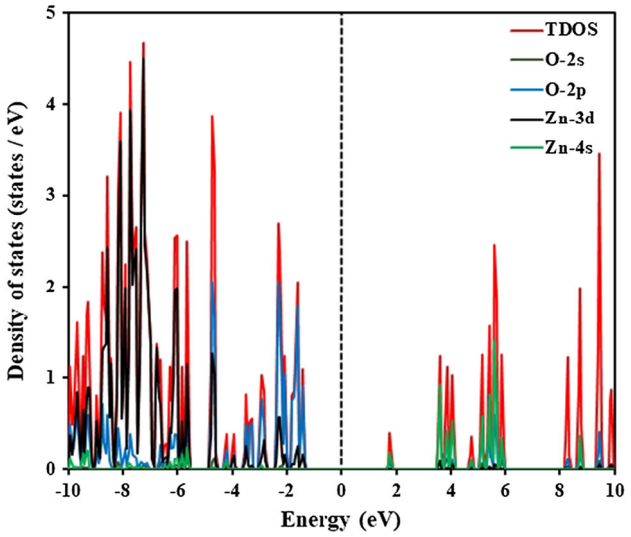

Fig. 13 The density of states for ZnO in the B2 structure at 170 GPa

Pma2 at 80th step and *Cmmm* at 85th step. These intermediary states are depicted in Fig. 6 for the evolution of the B1 structure and in Fig. 7 for the evolution of the B2 structure.

The calculated electronic band structures of ZnO are given in Figs. 8, 9 and 10 for B4, B1 and B2 structures along high symmetry directions and shown at the level of Fermi energy as a function of the energy. The Fermi energy level is set to 0 eV. The symmetry points are chosen as $\Gamma - M - K - \Gamma - A - L - H$ for the B1 phase, $\Gamma - X - W - \Gamma - L - W - L - X$ for the B1 phase and $X - R - M - \Gamma - R$ for the B2 phase. As seen from the electronic band structure graphs, the valence band is located below the Fermi energy level and the transmission band is located on the top. The obtained results show that ZnO at 0 GPa corresponds to a direct band transition with a band gap of about 0.69 eV. Because the maximum of the valence band and the minimum of the conduction band are at the same symmetry point [Γ]. $Fm\bar{3}m$ and $Pm\bar{3}m$ phases of ZnO correspond to indirect band transition with a band gaps of 1.99 and 0.98 eV, respectively. Thus, all phases of ZnO show semiconductor characteristic.

It also calculated the density of states (DOS) to obtain further information about the electronic nature of ZnO and depicted in Figs. 11, 12 and 13. It can be seen from these figures that the largest contribution came from Zn-3d state below the Fermi energy level and from Zn-4s above the Fermi energy level for all phases of ZnO.

Elastic constants (C_{ij}) are the important properties of solids, which determine the mechanical stability of crystals. So, we also calculated the elastic constants to investigate the mechanical stability of the obtained phases of ZnO. The obtained C_{ij} values are given in Table 3. The well-known conditions for the mechanical stability of hexagonal and cubic structures are: $C44 > 0$, $C_{11} > |C_{12}|$, $(C_{11} + 2C_{12})C_{33} > 2C_{13}^2$ for hexagonal and $C_{11} > 0$, $C_{44} > 0$, $C_{11} > |C_{12}|$, $(C_{11} + 2C_{12}) > 0$ for cubic [39–41]. Our results given in Table 3 satisfy these stability conditions for $P6_3mc$ and $Fm\bar{3}m$ phases of ZnO. So, these phases are mechanically stable. However, the $Pm\bar{3}m$ phase of ZnO is mechanically unstable because it does not provide the conditions of cubic stability.

The calculated phonon dispersion curves for the B4 and B1 structures of ZnO are shown in Figs. 14 and 15, respectively. Since unit cell of the $P6_3mc$ phase of ZnO contains four atoms, the corresponding number of vibration modes is twelve, as seen in Fig. 14, of which three are acoustic branches and the remaining nine are optical modes. The $Fm\bar{3}m$ phase of ZnO contains eight atoms; the corresponding number of vibration modes is twenty four,

Table 3 Elastic constants (in GPa) for ZnO in $P6_3mc$, $Fm\bar{3}m$, and $Pm\bar{3}m$ phases

Phases	C_{11}	C_{12}	C_{13}	C_{33}	C_{44}	References
$P6_3mc$	192.32	109.04	92.21	204.07	41.62	This study
	221	139	124	238	38	[10]
	235.007	66.742	60.95	287.891	49.891	[42]
	206	118	118	211	44	[43]
	190	110	90	196	39	[44]
$Fm\bar{3}m$	229.45	139.35			83.82	This study
	305	159			129	[9]
	278	172			87	[10]
	237	145			82	[42]
	326	139			110	[45]
$Pm\bar{3}m$	462.98	47.167			− 56.261	This study
	477	68			− 68	[10]
	433.76	35.975			69.041	[42]

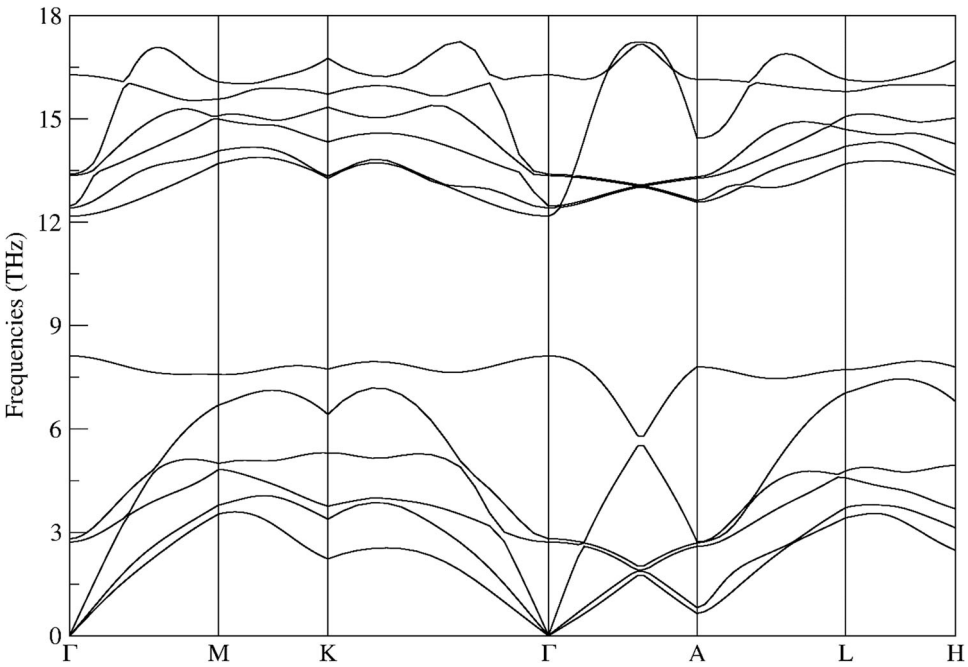

Fig. 14 The phonon dispersion curves for ZnO in the B4 structure at 0 GPa

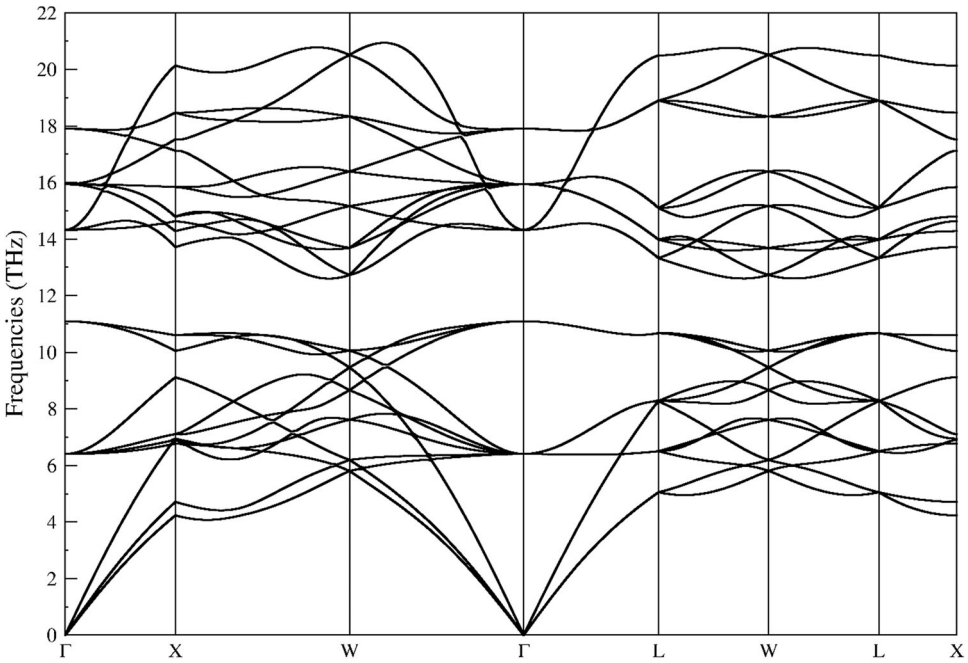

Fig. 15 The phonon dispersion curves for ZnO in the B1 structure at 30 GPa

as seen in Fig. 15, of which three are acoustic branches and the remaining twenty one are optical modes. We do not find any imaginary phonon frequency in the whole Brillouin zone for the $P6_3mc$ and $Fm\bar{3}m$ phase of ZnO. This supports the dynamical stability of $P6_3mc$ and $Fm\bar{3}m$ phase of ZnO. As can be seen from the elastic constant calculations, since the $Pm\bar{3}m$ phase of ZnO is mechanically unstable, we did not make the phonon calculate for the $Pm\bar{3}m$ phase. The $Pm\bar{3}m$ phase of ZnO is also dynamically unstable.

4. Conclusions

We investigated phase transition properties of ZnO under high hydrostatic pressure using ab initio calculations. ZnO exhibits phase transition at different pressures. The phase

transformations from the B4 structure with space group $P6_3mc$ to the B1 structure with space group $Fm\bar{3}m$ and from this B1 structure to the B2 structure with space group $Pm\bar{3}m$ were obtained at 9 and 119.5 GPa, respectively. In addition, five and six intermediate states for the first time were predicted in the simulations for ZnO. Therefore, the analysis of phase transition properties implies that ZnO considerably shows a dependence on the composition under pressure. Also, we studied electronic, elastic and vibrational properties of ZnO and obtained band gaps from band structure about 0.69, 1.99 and 0.98 eV for $P6_3mc$, $Fm\bar{3}m$ and $Pm\bar{3}m$ phases, respectively.

References

[1] L Stolt, J Hedström, J Kessler, M Ruckh, K O Velthaus and H W Schock *Appl. Phys. Lett.* **62** 597 (1993)
[2] T Ikeda, K Sato, Y Hayashi, Y Wakayama, K Adachi and H Nishimura *Solar Energy Mater. Solar Cells* **34** 379 (1994)
[3] Z Xin-Yu, C Zhou-Wen, Q Yan-Peng, F Yan, Z Liang, Q Li, M Ming-Zhen, L Ri-Ping and W Wen-Kui *Chin. Phys. Lett.* **24** 1032 (2007)
[4] A Schleife, F Fuchs, J Furthmüller and F Bechstedt *PhRvB* **73** 245212 (2006)
[5] F S Saoud, J C Plenet and M Henini *J. Alloys Compd.* **619** 812 (2015)
[6] X Dong, F Liu, Y Xie, W Shi, X Ye and J Z Jiang *Comput. Mater. Sci.* **65** 450 (2012)
[7] D Zagorac, J Schön, J Zagorac and M Jansen *PhRvB* **89** 075201 (2014)
[8] C Pu, X Tang and Q Zhang *Solid State Commun.* **151** 1533 (2011)
[9] Y Saeed, A Shaukat, N Ikram and M Tanveer *JPCS* **69** 1676 (2008)
[10] F-G Kuang, X-Y Kuang, S-Y Kang, M-M Zhong and A-J Mao *Mater. Sci. Semicond. Process.* **23** 63 (2014)
[11] B Amrani, I Chiboub, S Hiadsi, T Benmessabih and N Hamdadou *Solid State Commun.* **137** 395 (2006)
[12] D Maouche, F S Saoud and L Louail *MCP* **106** 11 (2007)
[13] S Cui, W Feng, H Hu, Z Feng and Y Wang *J. Alloys Compd.* **476** 306 (2009)
[14] J Recio, M Blanco, V Luana, R Pandey, L Gerward and J S Olsen *PhRvB* **58** 8949 (1998)
[15] H Karzel, W Potzel, M Köfferlein, W Schiessl, M Steiner, U Hiller, G Kalvius, D Mitchell, T Das and P Blaha *PhRvB* **53** 11425 (1996)
[16] J Jaffe and A Hess *Phys. Rev. B* **48** 7903 (1993)
[17] J E Jaffe, J A Snyder, Z Lin and A C Hess *Phys. Rev. B* **62** 1660 (2000)
[18] C H Bates, W B White and R Roy *Science* **137** 993 (1962)
[19] J C Jamieson *Phys. Earth Planet. Inter.* **3** 201 (1970)
[20] S Yu, I Spain and E Skelton *Solid State Commun.* **25** 49 (1978)
[21] S Desgreniers *Phys. Rev. B* **58** 14102 (1998)
[22] F Decremps, J Zhang and R Liebermann *EPL (Europhys. Lett.)* **51** 268 (2000)
[23] F Decremps, J Zhang, B Li and R C Liebermann *Phys. Rev. B* **63** 224105 (2001)
[24] R Ahuja, L Fast, O Eriksson, J Wills and B Johansson *J. Appl. Phys.* **83** 8065 (1998)
[25] S Saib and N Bouarissa *Physica Status Solidi (b)* **244** 1063 (2007)
[26] P Ordejón, E Artacho and J M Soler *Phys. Rev. B* **53** R10441 (1996)
[27] J P Perdew, K Burke and M Ernzerhof *Phys. Rev. Lett.* **77** 3865 (1996)
[28] N Troullier and J L Martins *PhRvB* **43** 1993 (1991)
[29] H J Monkhorst and J D Pack *PhRvB* **13** 5188 (1976)
[30] R Hundt, J C SchoÈn, A Hannemann and M Jansen *J. Appl. Crystallogr.* **32** 413 (1999)
[31] A Hannemann, R Hundt, J Schön and M Jansen *J. Appl. Crystallogr.* **31** 922 (1998)
[32] C Yamcicier, Z Merdan and C Kurkcu *Can. J. Phys.* **96** 216 (2017)
[33] C Kürkçü, A Selgin, Z Merdan, Ç Yamçiçier and H Öztürk *Chin. J. Phys.* **56** 783 (2018)
[34] M Durandurdu *Chem. Phys.* **369** 55 (2010)
[35] C Kürkçü, Z Merdan and H Öztürk *Russ. J. Phys. Chem. A* **90** 2550 (2016)
[36] C Kürkçü, Z Merdan and H Öztürk *Solid State Commun.* **231** 17 (2016)
[37] F Murnaghan *Proc. Natl. Acad. Sci.* **30** 244 (1944)
[38] F Birch *Phys. Rev.* **71** 809 (1947)
[39] A Candan and G Uğur *Mod. Phys. Lett. B* **30** 1650002 (2016)
[40] N Arikan, M Ersen, H Ocak, A İyigör, A Candan, Ş Uğur, G Uğur, R Khenata and D Varshney *Mod. Phys. Lett. B* **27** 1350224 (2013)
[41] A Candan and M Kurban *Solid State Commun.* **281** 38 (2018)
[42] M Kalay, H H Kart, S Özdemir Kart and T Çağın *J. Alloys Compd.* **484** 431 (2009)
[43] G Carlotti, D Fioretto, G Socino and E Verona *J. Phys.: Condens. Matter* **7** 9147 (1995)
[44] T Azuhata, M Takesada, T Yagi, A Shikanai, S F Chichibu, K Torii, A Nakamura, T Sota, G Cantwell, D B Eason and C W Litton *J. Appl. Phys.* **94** 968 (2003)
[45] Z Charifi, H Baaziz and A Hussain Reshak *Physica Status Solidi (b)* **244** 3154 (2007)